Submitted to the 29th International Conference on High-Energy Physics,
Vancouver, Canada July 1998

Double Diffraction Dissociation at large $|t|$ in Photoproduction at HERA

H1 Collaboration

Abstract

The double dissociation photoproduction cross section for the process $\gamma p \to XY$ is measured for the first time at large 4-momentum transfer squared $|t| > 20\mathrm{GeV}^2$. The systems X and Y are separated by the largest rapidity gap in the event with all particles on the photon side of the gap ascribed to the system X. Diffractive events are then characterised by $M_X, M_Y \ll W$, where W is the γp centre of mass energy. Cross sections are measured differentially in $x_{I\!P} = (M_X^2 - t)/W^2$, for $y_{I\!P} = (M_Y^2 - t)/W^2 < 0.018$. In the range $0.0007 < x_{I\!P} < 0.0040$, the shape of the measured $x_{I\!P}$ distribution is compared to predictions for standard photoproduction processes and to a model based on the exchange of a strongly interacting colour singlet object at large $|t|$.

Abstract 570
Parallel Sessions 5,3
Plenary Sessions 7,5

1 Introduction

In recent years much effort, both experimental and theoretical, has been focused on the class of diffractive processes in which the square of the four momentum transfer across the rapidity gap, $-t$, is large. In this case, the rapidity gap producing mechanism is driven by short distance physics [1], and consequently perturbative QCD calculations are possible. Calculations of elastic parton-parton scattering have been performed using the leading logarithmic approximation (LLA) of BFKL [2]. Experimentally, such processes have been studied in the form of the 'rapidity gaps between jets' process suggested by Mueller & Tang [3] and measured at the TEVATRON [4, 5] and HERA [6]. In this process the fraction of dijet events with a rapidity gap between the jet edges is measured as a function of the rapidity separation, $\Delta\eta$, between the jets. Whilst a signal for a gap producing mechanism above the expectation from normal pQCD processes is certainly observed, the approach falls short of providing a precise quantitative test of the theory. The requirement that two jets are observed in the detector severely restricts the accessible gap size, and since the BFKL cross section is predicted to rise exponentially with $\Delta\eta$, this is a major drawback. Furthermore, with the completion of the (large) next to leading logarithmic corrections to BFKL [7], the need for a well defined hadron level cross section measurement is all the more pressing, in order to really test the theory. At HERA, measurements of high $|t|$ vector meson production [8, 9] have provided access to larger rapidity gaps in a well defined kinematic range, although the rate is low. With this in mind, Cox and Forshaw [10] recently suggested the study of the more inclusive double dissociative process $\gamma p \to XY$ at high $|t|$. In this paper we report the first measurement of this process, based on H1 data taken during 1996.

The photon and proton dissociative systems, X and Y respectively, are separated by finding the largest rapidity gap in the event (the procedure used by the H1 Collaboration in previous diffractive measurements [11]). The process, shown schematically in figure 1, is considered in terms of the kinematic variables

$$W^2 = (\gamma + P)^2 \quad t = (P - Y)^2 \quad x_{I\!P} = \frac{\gamma.(P - Y)}{\gamma.P} \quad y_{I\!P} = \frac{P.(\gamma - X)}{\gamma.P} \tag{1}$$

where γ, P, X and Y are the 4-vectors of the photon, proton and X and Y systems respectively. W is the γP center of mass energy and t is the four momentum transfer across the rapidity gap. In this study we present measurements of the differential cross section $\mathrm{d}\sigma/\mathrm{d}x_{I\!P}(\gamma P \to XY)$ in the range $|t| > 20\mathrm{GeV}^2$, $165 < W < 233$ GeV, $0.0007 < x_{I\!P} < 0.0040$, $y_{I\!P} < 0.018$.

2 The H1 Detector

A detailed description of the H1 apparatus can be found elsewhere [12]. The following briefly describes the detector components relevant to this analysis.

A liquid argon (LAr) calorimeter [13] covers the range in polar angle $4° < \theta < 153°$ with full azimuthal coverage, where θ is defined with respect to the proton beam direction ($+z$ axis). The LAr consists of an electromagnetic section with lead absorbers and a hadronic section with steel absorbers, of combined depth between 4.5 and 8 interaction lengths. Both sections are highly segmented in the transverse and longitudinal directions with about 44000 cells in total. The absolute energy scale is known to 4% for hadronic energies. The polar region $153° < \theta < 177.8°$ is covered by the SPACAL [14], a lead / scintillating fibre calorimeter with both hadronic and electromagnetic sections. The hadronic energy scale uncertainty is presently 7%. Tracking information is provided by the two concentric drift chambers of the central tracker, covering the pseudo-rapidity range $-1.5 < \eta < 1.5$, which lie inside a 1.15 T solenoidal field.

The luminosity is measured from the reaction $ep \to ep\gamma$ with two TlCl/TlBr crystal calorimeters [12] installed in the HERA tunnel. The electron tagger is located at $z = -33$ m from the interaction point in the direction of the outgoing lepton beam and the photon tagger at $z = -103$ m.

3 Simulations

The HERWIG 5.9 [15] Monte Carlo event generator was used to correct the data for detector acceptance and bin migration effects. HERWIG incorporates the BFKL LLA colour singlet exchange cross section for the elastic scattering of two partons as computed by Mueller & Tang [3]. For the elastic scattering of a pair of quarks, carrying momentum fraction x_i of beam particle i, in the asymptotic limit $x_\gamma x_h W^2 \gg -t$, the cross section $\hat{\sigma}$ is

$$\frac{\mathrm{d}\hat{\sigma}(qq \to qq)}{\mathrm{d}t} = (\alpha_s C_F)^4 \frac{2\pi^3}{t^2} \frac{e^{2\omega_0 Y}}{(7\alpha_s N_c \zeta(3) Y)^3} \qquad (2)$$

where

$$Y = \ln\left(\frac{x_\gamma x_h W^2}{-t}\right)$$

$$\omega_0 = N_c \, 4\ln 2 \, \frac{\alpha_s}{\pi}$$

and N_c is the number of colours, ζ is the Riemann zeta function and C_f is the colour factor.

In all our plots, we use the exact leading logarithm expression which is not as yet available in the HERWIG 5.9 release [16]. The values of α_s in equation (2) are free parameters in the LLA, and are chosen to be 0.17.[1] This corresponds to a choice of $\omega_0 = 0.45$.

A sample of standard HERWIG direct and resolved photoproduction was also generated and mixed with the LLA BFKL sample, according to the generated luminosities. All HERWIG simulations use the GRV-HO parton distributions for the photon and proton [17]

4 Experimental Method

4.1 Event Selection

The data for this analysis were collected with the H1 detector during the 1996 running period, when HERA collided 27.6 GeV positrons with 820 GeV protons, with an integrated luminosity of 6.7 pb^{-1}. Photoproduction events were selected by detecting the scattered positron in the electron tagger. This restricts the virtuality of the photon to $Q^2 < 0.01$ GeV^2. The photon - proton centre of mass energy is restricted to the range $165 < W < 233$ GeV to avoid regions of low electron tagger acceptance.

The events were triggered by 2 independent triggers, one based on tracking requirements in the central tracker, the other on transverse electromagnetic energy in the SPACAL calorimeter. Each trigger was used to determine the efficiency of the other, and these efficiencies were combined and used in the cross section determination.

[1] Note that only 2 of the 3 α_s values in equation (2) are actually independent, however. Both values in the fraction should be the same, whereas α_s in the pre-factor may take a different value.

4.2 Reconstruction of $x_{\mathbb{P}}$, $y_{\mathbb{P}}$ and t

The reconstruction of the X and Y system 4-vectors has been optimised by combining tracking and calorimeter information. Techniques are applied to minimise the effects of detector noise. Precise details can be found elsewhere [11]. Losses in the forward and backward directions are, however, unavoidable, making the measurement of the invariant masses of the systems problematic. For this reason, we introduce the kinematic variables $x_{\mathbb{P}}$ and $y_{\mathbb{P}}$, reconstructed using the expressions

$$x_{\mathbb{P}} \simeq \frac{M_X^2 - t}{W^2} \simeq \frac{\Sigma(E+p_z)_X}{2E_p} \tag{3}$$

$$y_{\mathbb{P}} \simeq \frac{M_Y^2 - t}{W^2} \simeq \frac{\Sigma(E-p_z)_Y}{2E_\gamma} \tag{4}$$

where E_p and E_γ are the proton and photon beam energies respectively, and the quantity $\Sigma(E+p_z)_X$ ($\Sigma(E-p_z)_Y$) is summed over all hadrons reconstructed backward (forward) of the largest rapidity gap in the event. This quantity has the property that it is insensitive to losses down the beam pipe, for which $E \simeq -p_z$ ($E \simeq +p_z$). Figure 2 shows the correlation between the reconstructed and generated values of $x_{\mathbb{P}}$ and $y_{\mathbb{P}}$ in the HERWIG simulation. $x_{\mathbb{P}}$ is particularly well reconstructed for all values in the measurement. This is due to the large Lorentz boost of the CMS system, which draws the X system into the main calorimeters. In the case of $y_{\mathbb{P}}$, the opposite is true, and measurements corresponding to low values of M_Y are not possible. For these events, however, the reconstructed $y_{\mathbb{P}}$ tends to underestimate the true value, and such events therefore do not migrate out of the sample. For $y_{\mathbb{P}} > 0.018$ an accurate $y_{\mathbb{P}}$ reconstruction becomes possible, such that migrations into the sample from large $y_{\mathbb{P}}$ are well controlled.

In order to ensure that the systems X and Y are clearly separated, only events with a rapidity gap between the two systems of at least 1.5 units of rapidity are selected. These events are specified by $M_X, M_Y \ll W$, and hence our sample is defined in the kinematic range $y_{\mathbb{P}} < 0.018$ and $0.0007 < x_{\mathbb{P}} < 0.0040$.

The reconstruction of t is more problematic. It is measured as the negative squared transverse momentum of the X system, $-(p_t)_X$, and is sensitive to losses down the backward beam pipe, particularly for low values of $|t|$. For this reason we choose to define our sample for $|t| > 20\mathrm{GeV}^2$.

4.3 Extraction of the cross section and error analysis

The events selected by the criteria described in sections 4.1 and 4.2 are used to determine the cross section $d\sigma/dx_{\mathbb{P}}(\gamma P \to XY)$ in the kinematic range defined in section 1. The HERWIG simulation described in section 3 is used to correct for losses and migration effects in $x_{\mathbb{P}}$, $y_{\mathbb{P}}$ and t. Of particular importance given the uncertainty in the measurement of t described in section 4.2 is the Monte Carlo simulation of the t distribution. This is shown in figure 3 (a). A good description of the data is seen down to the lowest relevant t values, and this gives us confidence that the t migrations are correctly accounted for in the correction procedure. Also shown in figure 3 (b) is the percentage resolution in t in the HERWIG generator sample. Although there is a significant tail in this distribution, we find that the percentage of events in each $x_{\mathbb{P}}$ bin which migrate into the sample from below $|t| = 20$ GeV is under 30% in each $x_{\mathbb{P}}$ bin, and remains approximately constant from bin to bin. Any losses due to the rapidity gap cut described in section 4.2 are included in the acceptance corrections [2]. The upper and lower edges of the

[2] Note that the requirement that the rapidity separation between the X and Y systems must be > 1.5 is NOT part of the hadron level cross section definition

rapidity gap are shown in figures 4 (a) and (b) respectively. Again, HERWIG is seen to give a good description of the data.

Contributions to the statistical error come from the limited number of data events in the sample and the number of Monte Carlo events used to correct the data. These are added in quadrature.

Systematic uncertainties are calculated on a bin by bin basis, and added in quadrature. Two sources of systematic error dominate. The first is due to the limited number of data events available to calculate the trigger efficiency, contributing a systematic error of approximately 30% in each bin. The second comes from the Monte Carlo model dependence of the acceptance corrections. This systematic was estimated by re-weighting the t, $x_{I\!P}$ and $y_{I\!P}$ dependence of the generated distributions within sensible limits. The resulting systematic error was 30%. Other sources of systematic error are the uncertainties in the calorimeter energy scales, luminosity determination and electron tagger acceptance.

5 Results

The $x_{I\!P}$ distribution, corrected for detector effects, is shown in figure 5. The inner error bars are statistical and the outer error bars are the quadratic sum of the statistical and systematic errors. The solid line is the prediction from the HERWIG generator for all non-singlet exchange photoproduction processes. A significant excess above the expectation from the standard photoproduction model is observed. The dashed line shows the HERWIG prediction with the LLA BFKL prediction added. Good agreement is observed in both normalisation and shape. Care must be taken, however, in the interpretation of this result. There is a large theoretical uncertainty in the overall normalisation of the LLA BFKL cross section prediction shown in equation (2). The agreement in normalisation may well therefore be fortuitous. It should also be noted that the shape of the $x_{I\!P}$ distribution in this region of phase space is not only determined by the underlying dynamics of the interaction, but also by kinematic effects. There is a kinematic limit on the lowest possible value of $x_{I\!P}$, set by the requirement that $|t| > 20\text{GeV}^2$ and $165 < W < 233$ GeV, of $x_{I\!P} \simeq 7 \text{ x } 10^{-4}$ (see equation (3)). This forces the cross section down in the lowest $x_{I\!P}$ bin. The good agreement in shape with the BFKL Monte Carlo prediction, however, implies that the data are consistent with a value of $\omega_0 \simeq 0.45$ within this model.

Despite these limitations, however, with higher statistics the outlook for the future is promising. This measurement demonstrates that it is possible to extend greatly the reach in rapidity allowed by the gaps between jets approach. With the improved statistics already collected in the 1997 HERA running period, and higher luminosity in the future, a much more precise determination of the dependence of the cross section on $x_{I\!P}$ will be possible.

6 Acknowledgments

We are grateful to the HERA machine group whose outstanding efforts have made and continue to make this experiment possible. We thank the engineers and technicians for their work in constructing and now maintaining the H1 detector, our funding agencies for financial support, the DESY technical staff for continual assistance, and the DESY directorate for the hospitality which they extend to the non-DESY members of the collaboration.

References

[1] J.R.Forshaw and P.J.Sutton, Eur.Phys.J. C1 (1998) 285.

[2] E.A.Kuraev, L.N.Lipatov and V.S.Fadin, Sov.Phys.JETP 45 (1977) 199.
Ya.Ya.Balitsky and L.N.Lipatov, Sov.J.Nucl.Phys 28 (1978) 822.
L.N.Lipatov, Sov.Phys.JETP 63 (1986) 904.

[3] A.H.Mueller and W.-K.Tang, Phys.Lett. B284, (1992) 123.

[4] D0 Collaboration: S.Abachi et al., Phys.Rev.Lett. 72 (1994) 2332; Phys.Rev.Lett. 76 (1996) 734.
CDF Collaboration: F.Abe et al., Phys.Rev.Lett. 74 (1995) 855.

[5] K.Borras, for the CDF Collaboration, CDF/PUB/JET/PUBLIC/4590.
A. Brandt and J. Perkins, Proceedings from LISHEP98: LAFEX International School on High Energy Physics, Session C: Workshop on Diffractive Physics, Rio de Janeiro, Brazil, Feb. 1998.

[6] ZEUS Collaboration: M.Derrick et al., Phys.Lett. B369 (1996) 55.
H1 Collaboration: "Rapidity Gaps Between Jets in Photoproduction at HERA" contribution to The International Europhysics Conference on High Energy Physics, August 1997, Jerusalem, Israel.

[7] L.N.Lipatov and V.S.Fadin, Sov.J.Nucl.Phys. 50 (1989) 712; JETP Lett. 89 (1989) 352.
V.S.Fadin and R.Fiore, Phys.Lett. B294 (192) 286.
V.S.Fadin and L.N.Lipatov, Nucl.Phys. B406 (1993) 259; B477 (1996) 767; hep-ph/9802290.
V.S.Fadin, R.Fiore and A.Quartarolo, Phys.Rev. D50 (1994) 2265; D50 (1994) 5893; D53 (1996) 2729.
V.S.Fadin, R.Fiore and M.I.Kotsky, Phys.Lett. B387 (1996) 593; Phys.Lett. B359 (1995) 181.
V.S.Fadin, M.I.Kotsky and L.N.Lipatov, hep-ph/9704267.
V.S.Fadin et al., hep-ph/9711427.
G.Camici and M.Ciafaloni, Phys.Lett. B386 (1996) 341; Nucl.Phys. B496 (1997) 305.
M.Ciafaloni and G.Camici, Phys.Lett. B412 (1997) 396 and erratum; hep-ph/9803389.

[8] I.F.Ginzberg, S.L.Panfil and V.G.Serbo, Nucl.Phys. B284 (1987) 685.
J.R.Forshaw and M.G.Ryskin, Z.Phys. C68 (1995) 137.
J.Bartels, J.R.Forshaw, M.Wüsthoff and H.Lotter, Phys.Lett. B375 (1996) 301.
D.Yu.Ivanov, Phys.Rev. D53 (1996) 3564.
I.F.Ginzburg and D.Yu.Ivanov, Phys.Rev. D54 (1996) 5523.

[9] H1 Collaboration: "Production of J/Ψ Mesons with large $|t|$ at HERA" contribution to The International Europhysics Conference on High Energy Physics, August 1997, Jerusalem, Israel.
ZEUS Collaboration: "Study of Vector Meson Production at Large $|t|$ at HERA" contribution to The International Europhysics Conference on High Energy Physics, August 1997, Jerusalem, Israel.

[10] B. E. Cox and J. R. Forshaw, "Double Diffractive Dissociation at large t", MAN/HEP/98/2, MC/TH/98/7, hep-ph/9805206 to be published in Phys. Lett. B

[11] H1 Collaboration: C.Adloff et al., Z.Phys. C74 (1997) 221.

[12] H1 Collaboration; I. Abt et al., Nucl. Instr. and Meth. **A386** (1997) 310; 348.

[13] H1 Calorimeter Group; B. Andrieu et al., Nucl. Instr. and Meth. **A336** (1993) 460.

[14] H1 SPACAL group, R.D. Appuhn et al., Nucl. Instr. and Meth. **A386** (1997) 397.

[15] G.Marchesini et al., Comp.Phys.Comm. 67 (1992) 465.

[16] M.E.Hayes, Bristol University, PhD Thesis (1998).

[17] M. Glück, E. Reya, A. Vogt, Z. Phys. **C67** (1995) 433.

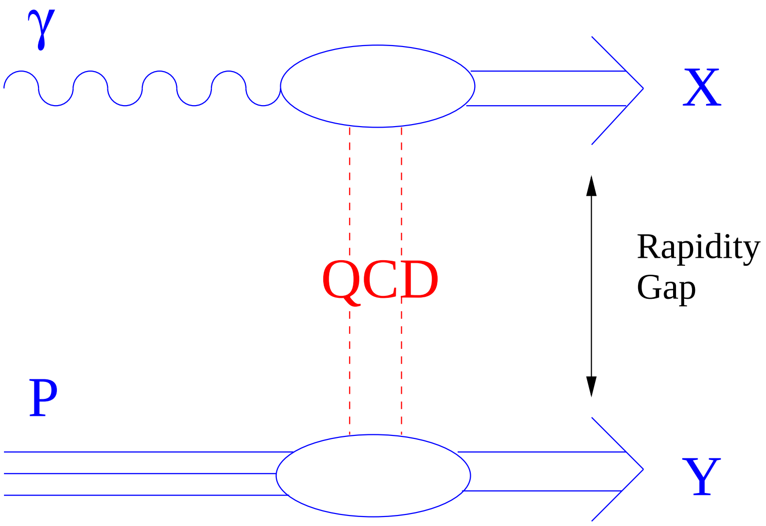

Figure 1: The double diffraction dissociation process at HERA.

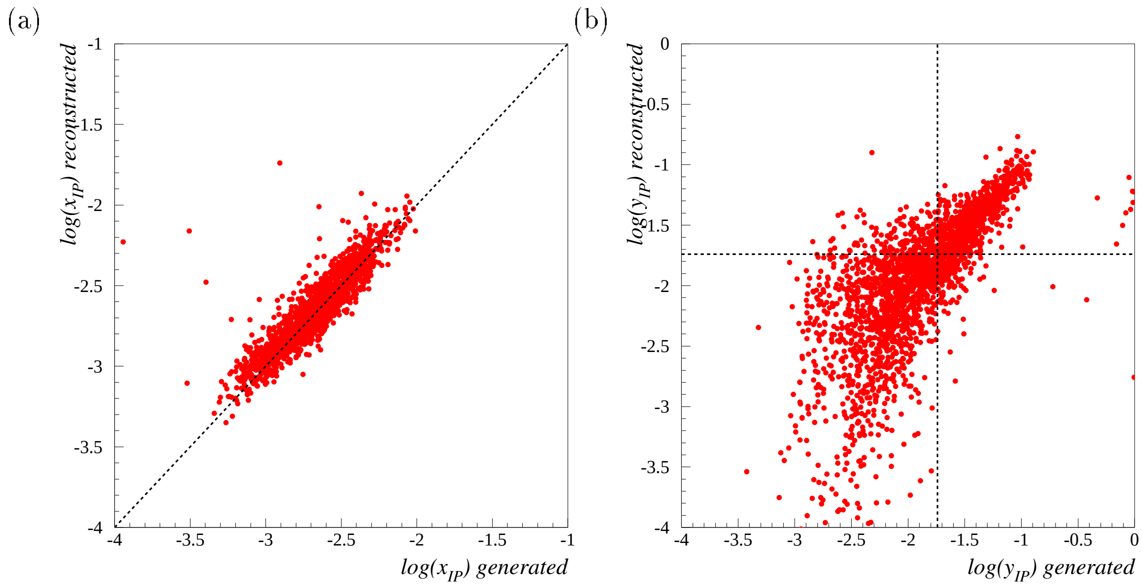

Figure 2: Correlation between reconstructed and generated values of (a) $x_{I\!P}$ and (b) $y_{I\!P}$ in the HERWIG simulation. The solid lines in (b) show the position of the kinematic cuts.

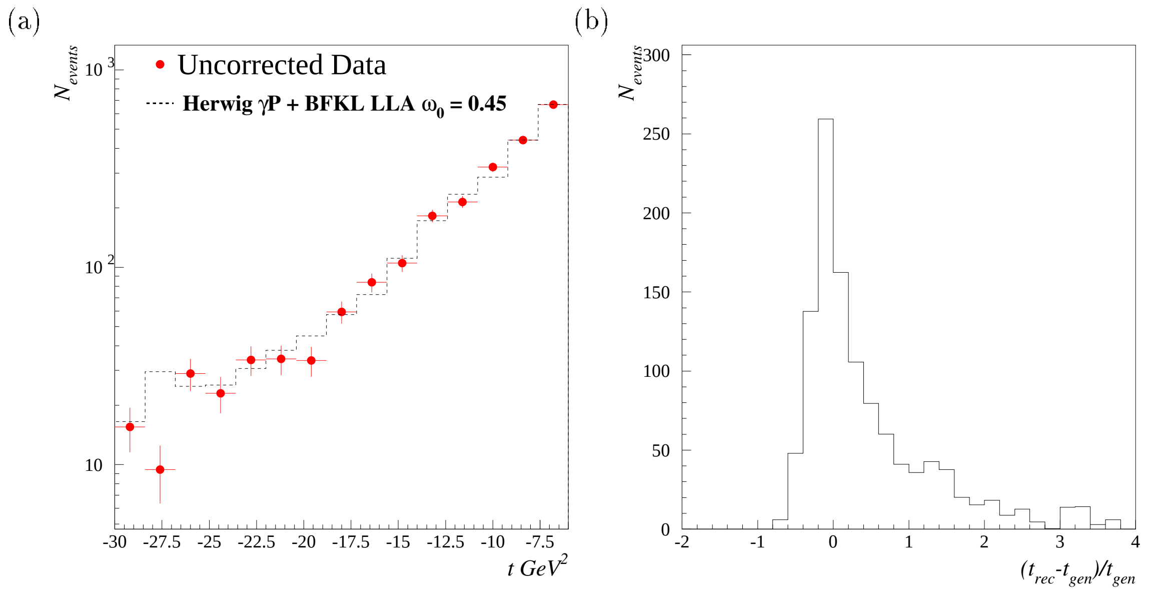

Figure 3: Comparison of the H1 data and HERWIG generator distributions for t (a) and the percentage resolution in t from the HERWIG generator sample (b).

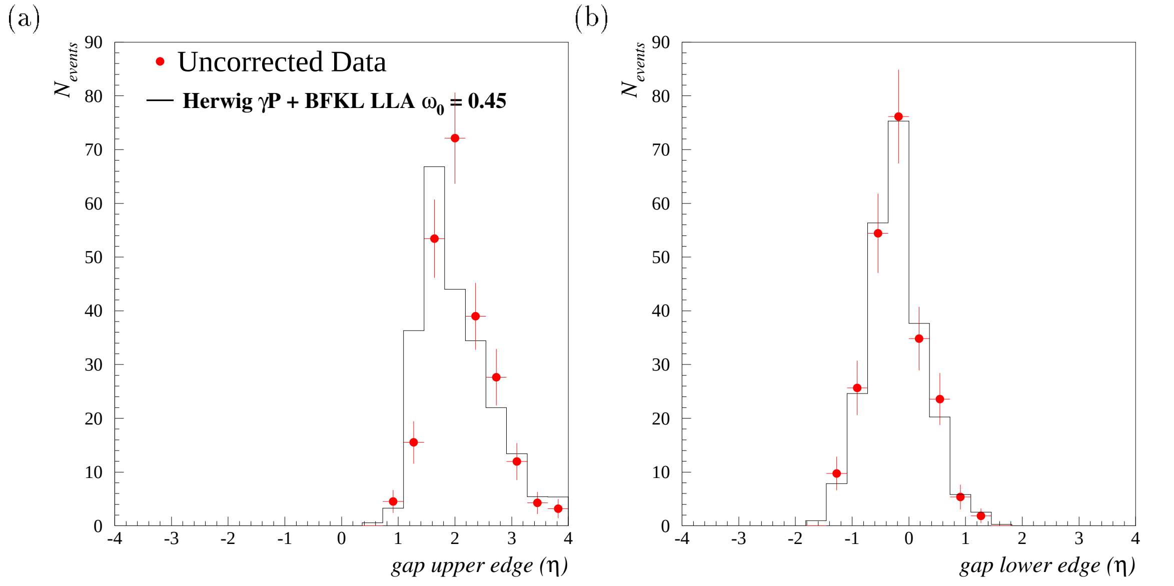

Figure 4: Comparison of the H1 data and HERWIG generator distributions for the upper (a) and lower (b) edges of the largest rapidity gap in the event as a function of $\Delta\eta$.

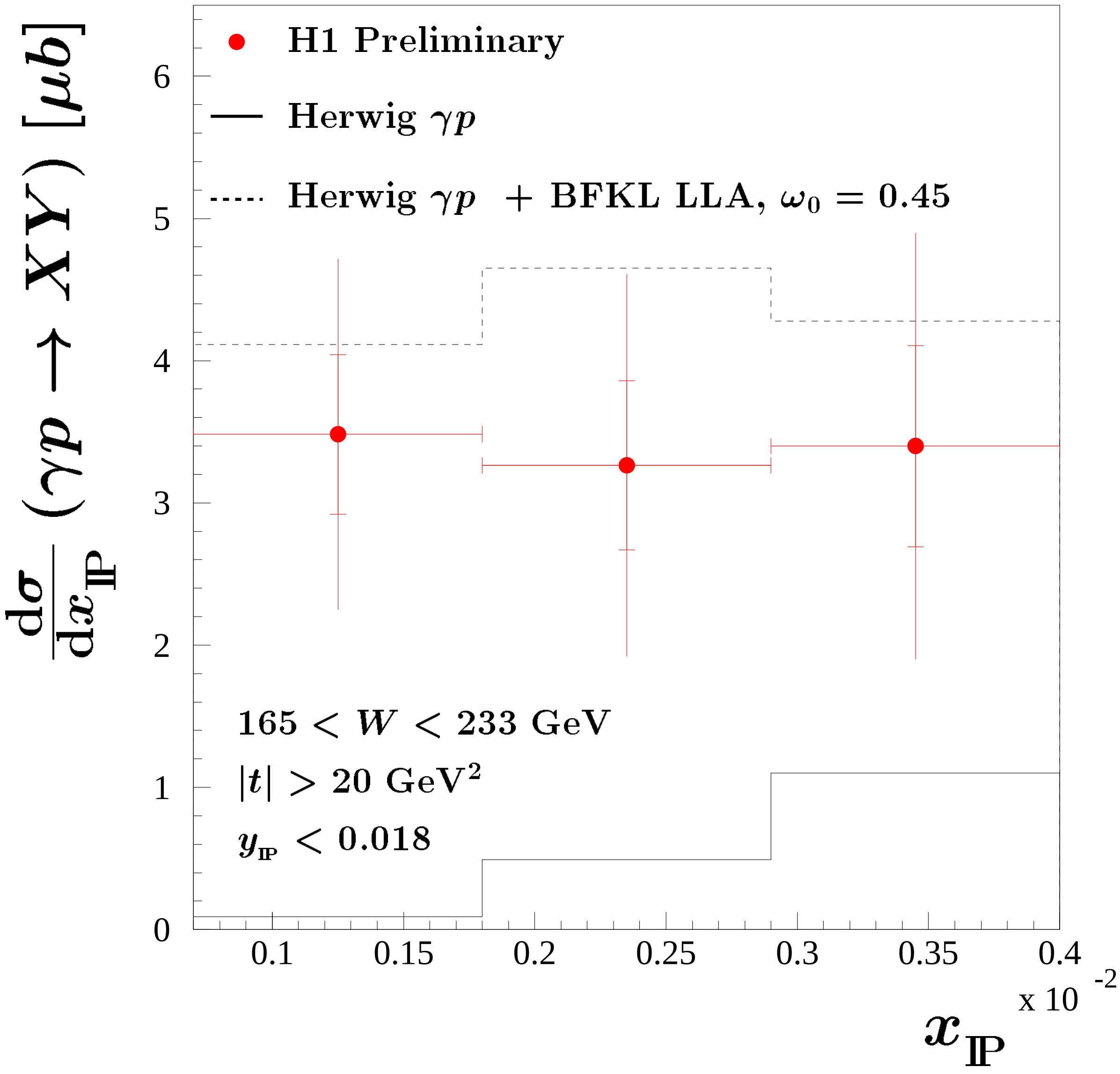

Figure 5: The differential cross section $\mathrm{d}\sigma/\mathrm{d}x_{\mathbb{P}}(\gamma P \to XY)$